

Exploring the central region of NGC 1365 in the ultraviolet domain

KSHAMA SARA KURIAN ^{1,2}, C. S. STALIN ¹, DOMINIKA WYLEZALEK ³, MARIYA LYUBENOVA ⁴,
TEK PRASAD ADHIKARI ^{5,6}, ASHISH DEVARAJ ⁷, RAM SAGAR ¹, MARKUS-KISSSLER PATIG ⁸, AND
SANTANU MONDAL ¹

¹*Indian Institute of Astrophysics, Koramangala, Block II, Bangalore 560034, India*

²*Pondicherry University, Kalapet, Puducherry 605014, India*

³*Astronomisches Rechen-Institut, Zentrum für Astronomie der Universität Heidelberg, Monchhofstr. 12-14, 69120 Heidelberg, Germany*

⁴*European Southern Observatory, Karl-Schwarzschild-Str. 2, 85748 Garching bei München, Germany*

⁵*CAS Key Laboratory for Research in Galaxies and Cosmology, Department of Astronomy, University of Science and Technology of China, Hefei, Anhui 230026, China*

⁶*School of Astronomy and Space Science, University of Science and Technology of China, Hefei, Anhui 230026, China*

⁷*Department of Physics and Electronics, CHRIST (Deemed to be University), Bangalore 560029, India*

⁸*ESA - ESAC - European Space Agency, Camino Bajo del Castillo s/n, 28692 Villafranca del Castillo, Madrid, Spain*

ABSTRACT

Active galactic nuclei (AGN) feedback and its impact on their host galaxies are critical to our understanding of galaxy evolution. Here, we present a combined analysis of new high resolution ultraviolet (UV) data from the Ultraviolet Imaging Telescope (UVIT) on *AstroSat* and archival optical spectroscopic data from VLT/MUSE, for the Seyfert galaxy, NGC 1365. Concentrating on the central 5 kpc region, the UVIT images in the far and near UV show bright star forming knots in the circumnuclear ring as well as a faint central source. After correcting for extinction, we found the star formation rate (SFR) surface density of the circumnuclear 2 kpc ring to be similar to other starbursts, despite the presence of an AGN outflow, as seen in [OIII] 5007 Å. On the other hand, we found fainter UV and thus lower SFR in the direction south-east of the AGN relative to north-west in agreement with observations at other wavelengths from JWST and ALMA. The AGN outflow velocity is found to be lesser than the escape velocity, suggesting that the outflowing gas will rain back into the galaxy. The deep UV data has also revealed diffuse UV emission in the direction of the AGN outflow. By combining [OIII] and UV data, we found the diffuse emission to be of AGN origin.

Keywords: galaxies: Seyfert — ultraviolet: galaxies — galaxies: evolution

1. INTRODUCTION

Most galaxies in the Universe harbour supermassive black holes (SMBHs; 10^6 – 10^{10} M_{\odot}) at their centres (Kormendy & Richstone 1995; Kormendy & Ho 2013). These SMBHs while accreting matter from their surroundings lead to the trigger of the active galactic nuclei (AGN) as well as the growth of the host galaxy. This close relationship between AGN and host galaxy is also evident in the correlation observed between the mass of the SMBH (M_{BH}) in AGN and galaxy luminosity (Kormendy & Richstone 1995), M_{BH} and galaxy mass (Magorrian et al. 1998) and M_{BH} and the velocity dis-

persion σ , of the stellar bulge (M- σ relation; Ferrarese & Merritt 2000). AGN thus play an important role in the evolution of galaxies via the injection of energy into the gas in their host galaxies, a process called feedback (Fabian 2012; King & Pounds 2015).

In many AGN, nuclear outflows from their central regions, in both ionized and molecular phases have been observed and these outflows can have a strong impact on the formation of stars in the central regions of AGN. They can either suppress star formation (negative feedback; Maiolino et al. 2012; Harrison 2017) or enhance star formation (positive feedback; Zubovas et al. 2013; Nesvadba et al. 2020). Also, both positive and negative feedback could operate in the same system (Shin et al. 2019; García-Bernete et al. 2021). A clear understanding of the impact AGN have on the central re-

gions of their host galaxies requires high-resolution observations such as those from integral field spectroscopy (IFS) which can spatially resolve star formation (SF) and AGN outflows. Such high-resolution observations have become possible in recent years. However, combining such high spatial resolution observations, along with observations at other wavelengths such as sub-mm/UV and photoionization modelling would be a robust and better approach to establishing how the connection between SF and AGN works. At low redshifts, dominated by Seyfert-type AGN, we can spatially separate the AGN-dominated regions from the SF-dominated regions. Here we report the results of one such study on a nearby AGN NGC 1365.

NGC 1365 is a low luminosity ($L_{bol} = 2 \times 10^{43}$ erg s^{-1}) Seyfert 1.8 type AGN at a distance of 18.6 Mpc (Alonso-Herrero et al. 2012; Lindblad 1999). At this distance, 1 arcsec corresponds to about 90 pc. An early comprehensive review of the characteristics of the AGN in NGC 1365, can be found in Lindblad (1999). It is found to show biconical ionised outflows in [OIII] (Phillips et al. 1983; Lena et al. 2016; Venturi et al. 2018). Star-forming clusters have also been found in the central regions of NGC 1365 from infrared observations (Alonso-Herrero et al. 2012; Fazeli et al. 2019; Whitmore et al. 2023; Liu et al. 2023) and X-ray studies (Wang et al. 2009). This source has been extensively studied at high spatial resolution in the optical using IFS data from VLT/MUSE (Venturi et al. 2018) and optical spectra from TYPHOON (Sextl et al. 2024), in the infrared using Herschel (Sandqvist et al. 2021), in the near and mid-infrared using JWST (Liu et al. 2023; Whitmore et al. 2023; Schinnerer et al. 2023) as well as in the sub-mm using ALMA (Gao et al. 2021; Schinnerer et al. 2023). Although NGC 1365 is well studied in nearly all wavelength domains, the UV domain is unexplored. We aim to fill this gap and explore the relation between the AGN outflow and SF in the central 5 kpc square region (hereafter referred to as the 'inner region') of the galaxy using spatially resolved optical IFS data and newly acquired UV data from the Ultra-Violet Imaging Telescope (UVIT) onboard *AstroSat* (Agrawal 2006; Singh 2022), which is India's first space based multi-wavelength astronomical observatory.

2. OBSERVATIONS

2.1. UVIT

NGC 1365 was observed using UVIT in two broad band filters namely F169M (FUV; $\lambda_{mean} = 1608$ Å, $\Delta\lambda = 290$ Å) and N279M (NUV; $\lambda_{mean} = 2792$ Å, $\Delta\lambda = 90$ Å) (Tandon et al. 2017). UVIT has a spatial resolution better than 1.5 arcsec and covers a field

of view of ~ 28 arcmin diameter. The observations (PI: G. Dewangan) were done in the photon counting mode with a default frame count rate of ~ 29 frames per second (Tandon et al. 2017). We downloaded the science-ready level-2 (L2) images that correspond to the OBSIDs A02_006T01_9000000776, A02_006T01_9000000802 and A02_006T01_9000000934 from the Indian Space Science Data Center (ISSDC), Bangalore. In the combined images from ISSDC, we found the exposure time to be lesser than the sum of the individual orbit-wise images. We, therefore, based our analysis on the reduced orbit-wise images. We first aligned the orbit-wise images using the Image Reduction and Analysis Facility (IRAF; Tody 1986) and combined those aligned orbit-wise images to create the combined images filter-wise. The net exposure times of the resulting images are 24905 seconds and 37833 seconds in F169M and N279M filters respectively. Astrometry on the combined images was carried out using the astrometry.net package (Lang et al. 2010). The UVIT position of the AGN matches within 0.7 arcsec of the *Gaia* position. For NGC 1365 observations, the background in FUV and NUV is $1 \times 10^{-4} cps/arcsec^2$ and $2.2 \times 10^{-4} cps/arcsec^2$ respectively. The top panel of Fig. 1 shows the composite image of NGC 1365 in FUV (blue) and NUV (red). Bright FUV and NUV knots of SF are seen in the inner region and the spiral arms. The bottom panel of Fig. 1 shows the zoomed view of the FUV and NUV flux maps of the inner region that covers the MUSE field of view.

2.2. MUSE

The MUSE optical IFU observations of NGC 1365 were acquired on 12 October 2014 under the program 094.B-0321(A) (PI: A. Marconi) Venturi et al. 2018). For our data analysis, we used the fully reduced, 4 ksec deep data cube of NGC 1365 which is available on the ESO archive. The MUSE field of view is $1' \times 1'$ with a 0.2 arcsec/pixel spatial sampling. The median seeing during the observations was about 0.76 arcsec (Venturi et al. 2018). The spectral window is 4750–9352 Å and the spectral binning is 1.25 Å/channel.

3. DATA ANALYSIS

3.1. MUSE

We analysed the MUSE data using a combination of our own *python* scripts and the *python* package MPDAF (MUSE Python Data Analysis Framework; Bacon et al. 2016). The central 2 arcsec nuclear region was not considered for further analysis as we are not interested in the broad line region of NGC 1365. To estimate the host galaxy kinematics, we fitted a single Gaussian to the Ca+Fe blend (MUSE resolution allows the blend to

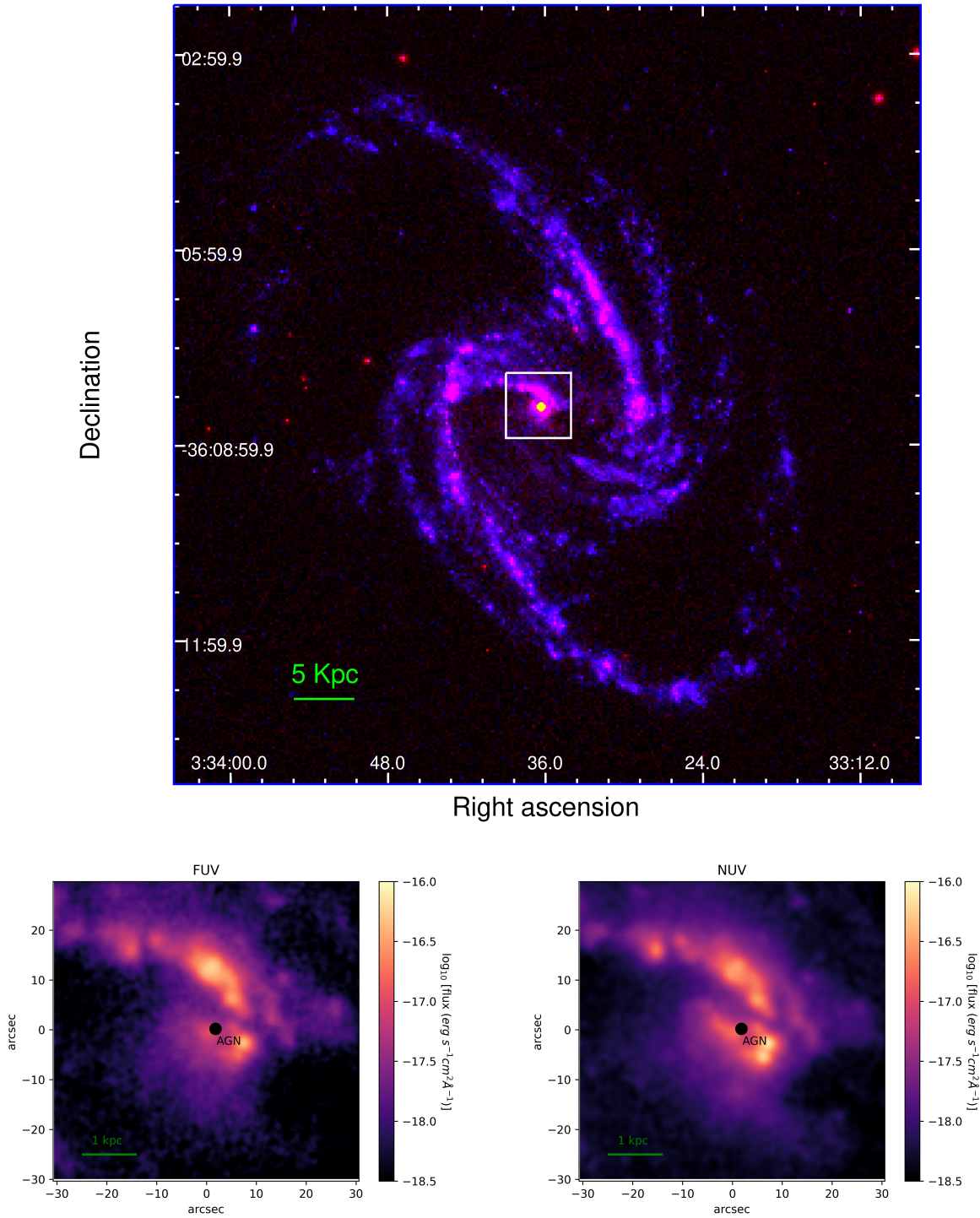


Figure 1. Top panel: Composite UVIT image of NGC 1365 with FUV in blue and NUV in red. The white box is the MUSE field of view ($\sim 1' \times 1'$) corresponding to the central 5 kpc region **which is the region analysed in this work**. The yellow dot in the centre of the box is the AGN position. Bottom panel: The UVIT FUV (left) and NUV (right) images of the inner **5 kpc** region of NGC 1365 **corresponding to the MUSE field of view**. They have been corrected for Milky Way extinction. The black dot in the centre of the NUV and FUV images is the AGN position.

be treated as a single line) at 6495 Å (Ho et al. 2009), after subtracting the stellar continuum. For this, spaxels with SNR (signal-to-noise ratio) > 3 were considered. Here, SNR is the ratio of the absolute value of the flux to the standard deviation of the line-free region of the continuum subtracted spectra. In the top left panel of Fig. 2 we show the rotational velocity of the inner region of NGC 1365 as derived from the Ca+Fe blend. This is similar to that derived by Venturi et al. (2018) using the Penalized PiXel Fitting (pPXF; Cappellari & Emsellem 2004) code.

We measure the flux of the [SII] doublet at 6716, 6731 Å, H β -[OIII] line complex (H β - 4861Å, [OIII] doublet - 4959, 5007Å) and H α -[NII] line complex (H α - 6564.6 Å, [NII] doublet - 6549.8, 6585.2 Å). To estimate the flux of the emission lines, we fitted **each individual** observed emission line with two Gaussian components (except for H β and H α which required an additional Gaussian component to account for the absorption line) that reproduces the line profile well. During the fit, the intensity ratios of the [OIII] and [NII] doublets were fixed to 2.95 and 3.0 respectively (Osterbrock & Ferland 2006). To separate shocked or Low-ionization nuclear emission-line (LINER) regions from AGN or Seyfert and starburst ionised gas, we used the [SII]-BPT (Baldwin, Phillips & Terlevich; Baldwin et al. 1981; Veilleux & Osterbrock 1987) diagram ([SII]6716,6731/H α vs [OIII]5007/H β). The BPT diagram indicates that the conical [OIII] 5007 Å emission seen in the inner region of NGC 1365 is predominately due to photoionization from AGN and is confined to the north-west (NW) and south-east (SE) directions.

We determined the kinematics of the [OIII] emission line using the V50 and W80 parameters (Zakamska & Greene 2014) from the total fitted line profile of the [OIII] 5007 Å line. The parameter V50 is the velocity at 50% of the total flux and is a proxy to the velocity shift. W80 is the difference between the 90th and 10th percentile of the total flux and is a proxy to the velocity dispersion (W80 = 1.088FWHM, Zakamska et al. 2016). Fig. 2 top right and bottom left panels show the kinematic maps derived from the [OIII] 5007 Å line. The AGN photoionized cone is clearly seen to be outflowing in the stellar rotational velocity subtracted [OIII] 5007 Å velocity shift map. The NW cone is red-shifted while the SE cone is blue-shifted. We found the AGN ionisation cone to have high W80 values of greater than 450 km/s.

We estimated the colour excess E(B-V) as

$$E(B - V) = 1.97 * \log_{10} \left[\frac{(H_{\alpha}/H_{\beta})_{obs}}{(H_{\alpha}/H_{\beta})_{int}} \right] \quad (1)$$

where $(H_{\alpha}/H_{\beta})_{obs}$ and $(H_{\alpha}/H_{\beta})_{int}$ is the observed and intrinsic H α /H β line ratio respectively. This equation considers an intrinsic value for (H_{α}/H_{β}) to be 2.87 under Case B recombination conditions (Osterbrock & Ferland 2006). Fig. 2 bottom right panel shows the E(B-V) map of the nebular gas. We found the ring to have an average E(B-V) of ~ 1 which translates to an A_v of ~ 3 (assuming $R_v = 3.1$) and is similar to that found by Venturi et al. (2018).

3.2. UVIT

The UVIT FUV and NUV images were converted to flux units using the unit conversion in Tandon et al. (2017). In order to perform a combined study of the MUSE and UVIT data, the UVIT FUV and NUV images of NGC 1365 were cropped to the MUSE field of view. The position of the AGN in UVIT matches with the MUSE position within 0.4 arcsec. We then corrected the UV data for the Galactic extinction using Cardelli et al. (1989), for a foreground extinction at the V band of 0.0543 mag, taken from Schlafly & Finkbeiner (2011). The intrinsic FUV and NUV fluxes were then estimated from the Milky Way corrected UV fluxes applying the Calzetti et al. (2000) reddening curve for the wavelength range, $1200 \text{ \AA} \leq \lambda \leq 6300 \text{ \AA}$, which is

$$k_{\lambda} = 2.65 \left(-2.15 + \frac{1.50}{\lambda} - \frac{0.19}{\lambda^2} + \frac{0.01}{\lambda^3} + R_v \right) \quad (2)$$

Here, $R_v = 3.1$. Following Calzetti et al. (2000), we estimated the colour excess of the stellar emission from the colour excess of the nebular emission using, $E_s(B - V) = 0.44E(B - V)$. We then calculated the intrinsic UV flux using the equation,

$$F_{int}(\lambda) = F_{obs}(\lambda) 10^{0.4E_s(B-V)k_{\lambda}} \quad (3)$$

4. RESULTS

4.1. UV slope- β

The UV continuum slope is a proxy to the UV colour from which age and other stellar population characteristics can be derived (Calzetti 2001). The UV slope β , is defined as the slope of the power law function, $F_{\lambda} \propto \lambda^{\beta}$ where F_{λ} is the flux density. We created a map of the observed and intrinsic (extinction corrected) UV slope, β which is shown in Fig. 3.

The intrinsic β map shows the star-forming regions in green with negative β values. The deepest green regions have β values close to -2.5 which is the dust free β value of a 5 Myr stellar population assuming an instantaneous burst of SF and solar abundance (refer to Table 6 in Calzetti 2001).

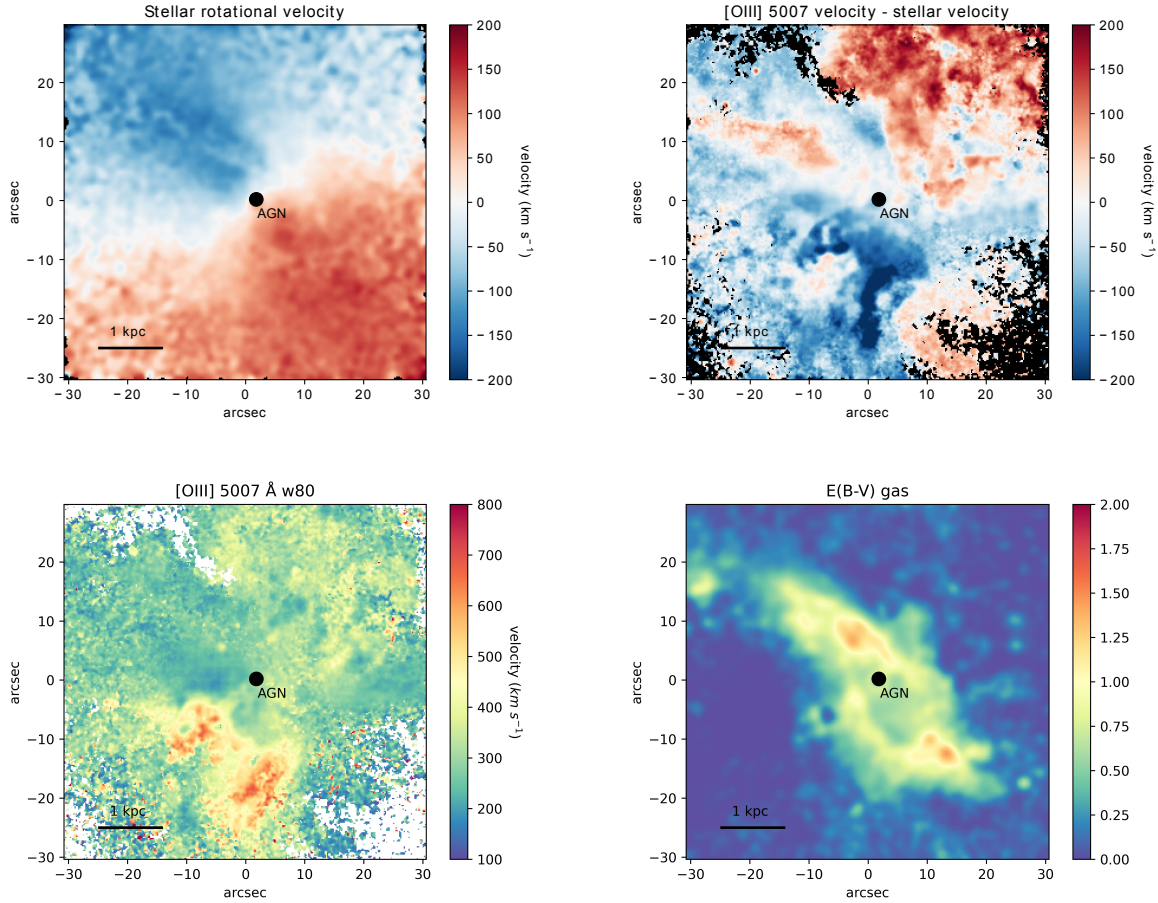


Figure 2. The stellar rotational velocity map (top left), the stellar rotational velocity subtracted [OIII] **5007 Å** velocity shift (top right), the W80 map of the [OIII] 5007 Å line (bottom left) and the E(B–V), of the nebular gas (bottom right). The AGN is marked based on the brightest H α region showing broad H α emission line width.

Table 1. SFR of the bright star-forming ring in the central region of diameter 2.2 kpc of NGC1365 ($r = 12''$, $1'' \sim 90$ pc, Kroupa IMF).

Attenuation law	SFR FUV $M_{\odot}\text{yr}^{-1}$	SFR NUV $M_{\odot}\text{yr}^{-1}$	SFR H α $M_{\odot}\text{yr}^{-1}$
Uncorrected	0.22	0.82	0.60
Starburst, $R_V = 3.1$	2.68	4.76	3.12
Starburst, $R_V = 4.05$	3.66	6.34	6.41
Milky Way	1.90	4.40	3.51
SMC	7.37	4.31	2.67

4.2. Star formation rate (SFR)

There are several SFR estimates in the literature, for the central regions of NGC 1365 (Gao et al. 2021; Fazeli et al. 2019; Alonso-Herrero et al. 2012). They mainly use H α flux values which is an indirect estimator of SFR. On the contrary, UV flux directly traces the radiation from young star-forming regions and thus is the most

appropriate estimator of SFR. Using the high-resolution extinction corrected UVIT FUV and NUV data, we derived new estimates of SFR. Most of the SF is said to be taking place in the Inner Lindblad region (Galliano et al. 2005), mainly concentrated in a star-forming ring of approximate diameter 2 kpc (Alonso-Herrero et al. 2012). We estimated the intrinsic FUV and NUV SFR for the central 12 arcsec radius region after masking the central 2 arcsec radius region which is dominated by AGN light (the 12 arcsec region is shown as a circle in Fig.7, left panel). We estimated the SFR using the following equation from Calzetti (2013), assuming a Kroupa IMF:

$$SFR = 3 \times 10^{-47} \lambda L_{\lambda} (M_{\odot}\text{yr}^{-1}) \quad (4)$$

The UV SFRs are highly dependent on extinction correction, and so, to be thorough, we estimated the SFR for Calzetti et al. (2000) reddening curve, with a starburst $R_V = 4.05$ and 3.1, the Small Magellanic Cloud (SMC) attenuation curve (Gordon et al. 2003) and the Milky Way reddening curve (Cardelli et al. 1989). For

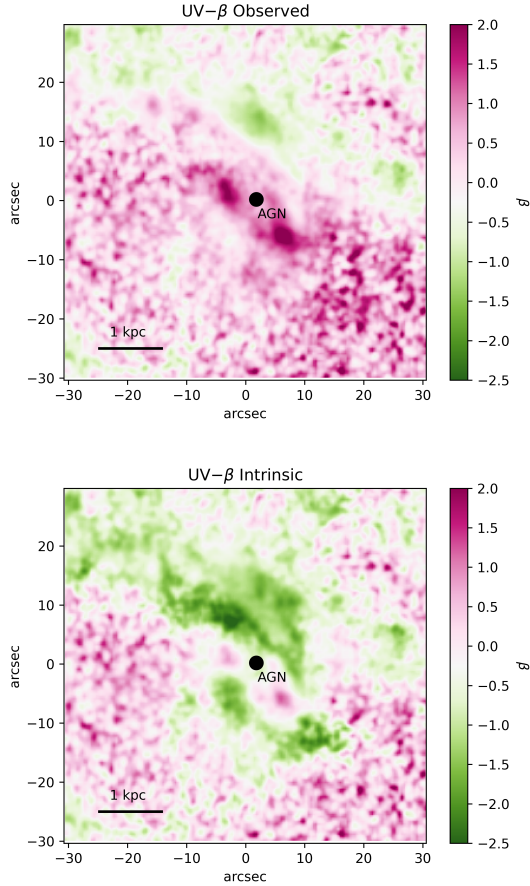


Figure 3. Map of the observed (top) and intrinsic (extinction corrected, bottom) UV slope, β of the inner region of NGC 1365. The extinction corrected β map shows negative β values (green coloured) in the regions predominantly occupied by **massive star formation** as seen in the $H\alpha$ map in Venturi et al. (2018).

comparison, we also estimated the SFR from $H\alpha$ flux values. Both the UV and $H\alpha$ SFRs are shown in Table 1. Alonso-Herrero et al. (2012) estimated an SFR of $5.6 M_{\odot}\text{yr}^{-1}$ from $H\alpha$ and Spitzer 24 micron IR flux, for a Salpeter IMF. We also derived the SFR surface density of NGC 1365 for a radius of 900 pc. It is found to be between 0.76 and $2.94 M_{\odot}/\text{yr}/\text{kpc}^2$ for SFR estimated from FUV and between 1.72 and $2.53 M_{\odot}/\text{yr}/\text{kpc}^2$ for SFR estimated from NUV, assuming the various attenuation curves. This is well within the expected SFR surface density at 1 kpc scale from the centre of the galaxy for other starbursts (Kennicutt 1998; Valencia-S. et al. 2012).

4.3. Spatial variation in SFR

In Fig. 4, we show the extinction corrected (following Calzetti et al. (2000) with $R_V = 3.1$) intrinsic FUV and NUV SFR map of the inner region with the [OIII] 5007 Å

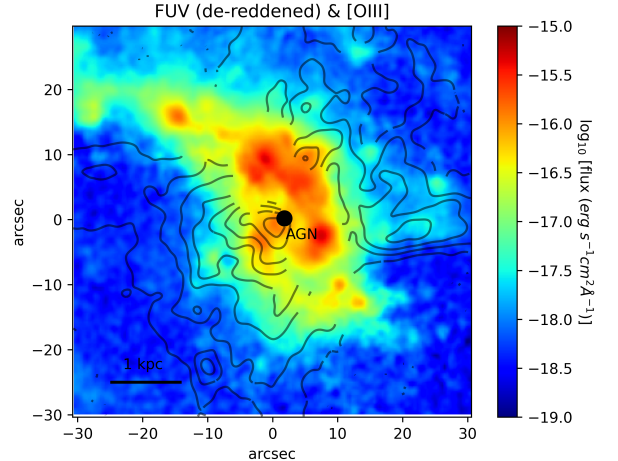


Figure 4. Extinction corrected, intrinsic UVIT FUV flux map of the inner region of NGC 1365, with MUSE [OIII] 5007 Å contours overlaid in black. Only the AGN-dominated regions are shown in the [OIII] contours after masking the LINER and starburst-dominated regions using the [SII]-BPT diagram.

AGN outflow contours overlaid in black. The starburst and LINER-dominated regions have been masked in the [OIII] outflow contours using the [SII]-BPT diagram and hence the [OIII] contours in this image show only the regions that are AGN-dominated.

The intrinsic UV flux maps are directly proportional to the spatially resolved SFR in the inner region. In NGC 1365, we found a spatial variation of SFR in the star-forming ring. Specifically, the SE part of the ring has low FUV (lower SFR) with respect to the NW side of the ring. The low SFR regions are co-spatial with the regions showing strong [OIII] contours in the SE cone possibly hinting at the outflow affecting the SF. However, star forming rings seen in galaxies are generally made of several aligned knots of SF and the SF can also be patchy (Comerón et al. 2010, 2014). Recently using high resolution observations of the inner region of NGC 1365 from ALMA and JWST coupled with simulations, Schinnerer et al. (2023) found that the distribution of SF in its central region is in-homogeneous. The northern side of the AGN has high SF, while the southern side has reduced SF, though the molecular gas is similar on both the northern and southern sides. According to them, the SF in the central region is driven by gas inflow via bar and SF in the southern regions has not yet started. They conclude that the AGN outflow has thus no impact on the gaseous disk. Considering the inclination of the AGN outflow and the galactic disk, the SE cone is above the disk with its axis 5° within the galaxy axis (Hjelm & Lindblad 1996). Hence it seems

less likely to intersect the galaxy plane. From studies of molecular gas kinematics, Liu et al. (2023) too do not find evidence of the ionized outflow to intersect the molecular gas disk. Recent high resolution observations are thus not in agreement with the scenario proposed by Gao et al. (2021) wherein the outflow impacts the molecular disk and causes AGN feedback, based on poor resolution ALMA maps. From UVIT observations, we found fainter UV and thus lower SFR in the SE side relative to the NW side of the AGN which is in agreement with the recent high resolution observations from JWST and ALMA (Schinnerer et al. 2023; Liu et al. 2023; Whitmore et al. 2023).

4.4. Diffuse UV light observed in the outflow cone

The UV morphology of the central regions of NGC 1365 predominantly points to a starburst origin of UV light when compared with the H α flux map. Along with the bright starburst regions, there is diffuse UV light in the NW and SE side of the AGN-dominated cone which is, in parts, similar to the morphology seen in the [OIII] outflow. This is shown in the Galactic extinction corrected UV images in the top panel of Fig. 5.

To determine the origin of this diffuse UV light, which is co-spatial with the [OIII] outflow region, we compared UV and [OIII] flux values to shock and photoionization models. We first calculated the flux ratios of FUV/[OIII], NUV/[OIII] and FUV/NUV for the outflow and the starburst ring of NGC 1365 after smoothing the [OIII] line emission map (by convolving with a Gaussian) to match the spatial resolution of UVIT data. To estimate the flux ratios, we used the Calzetti et al. (2000) ($R_V = 3.1$) extinction corrected FUV and NUV fluxes multiplied with their respective bandwidths ($\Delta\lambda = 290 \text{ \AA}$ for FUV and $\Delta\lambda = 90 \text{ \AA}$ for NUV). The starburst region was taken to be the same as the area used to determine the SFR in Section 4.2. This region was divided into smaller regions and the mean flux ratio in each section was calculated. The outflow region was roughly ascertained to be a double cone centred at the AGN, having a full opening angle of 90° , by using the [SII]-BPT AGN mask. This value of the opening angle is within the maximum opening angle of 100° modelled by Hjelm & Lindblad (1996).

We then estimated AGN and starburst photoionization as well as shock model flux ratios. The model values of the gas photoionized by AGN and starburst were generated using CLOUDY 17.0 (Ferland et al. 2017). For the AGN photoionization model, we considered a standard AGN continuum, with a big blue bump (BBB) temperature of 10^5K , an X-ray to UV slope of $\alpha_{ox} = -1.5$,

a low-energy BBB slope of $\alpha_{uv} = -0.5$, and an X-ray power-law index of $\alpha_x = -1.35$ (Guainazzi et al. 2009). We computed the AGN models under isobaric conditions assuming plane parallel geometry (Adhikari et al. 2018), with an initial pressure of $P = 2 \times 10^7 \text{ K}$ (D’Agostino et al. 2018). We adopted Milky Way dust grain abundance for solar metallicity. We generated a grid of spectra for photoionized gas, spanning a large range in ionisation parameters: $\log(U) = [-3.5, 2.0]$, hydrogen density $\log(n_H) = [3, 6]$ (these are typical densities of the AGN narrow line region) and total column density $\log(N_H) = [19, 24]$. For the starburst models, we generated spectra of spherical HII regions photoionized by instantaneous starburst continuum whose spectra with stellar masses that span the range between $1 M_\odot$ and $100 M_\odot$ were taken from Starburst99 (Leitherer et al. 1999) for ionisation parameter: $\log(U) = [-4.0, -2.0]$, hydrogen density $\log(n_H) = [1, 3]$ and starburst ages of 1 and 5 Myr. Similar to the AGN models, we adopted Milky Way dust grain abundance for solar metallicity for the starburst models.

The shock models were generated from MAPPINGS III (Allen et al. 2008) for shock velocities of 100 to 1000 km/s assuming pre-shock gas densities of $0.1\text{--}1 \text{ cm}^{-3}$ and magnetic field values of $1\text{--}10 \mu\text{G}$. We then compared the extinction corrected flux ratios (applying reddening curve by Calzetti et al. (2000), for an $R_V = 3.1$) to AGN photoionization, starburst photoionization and shock model predictions. Fig. 5 bottom panel shows the flux ratio map of FUV/[OIII] versus FUV/NUV and NUV/[OIII] versus FUV/NUV.

The flux ratios, FUV/[OIII] and NUV/[OIII], of the outflow region along with their FUV/NUV values are found to match with AGN models. This indicates that the diffuse UV emission in the outflow region is predominantly of AGN origin. This could be due to line emission from AGN photoionization of gas clouds in the outflow (Feltre et al. 2016) as well as direct and scattered AGN continuum light from electrons or dust in the outflow (Zakamska et al. 2005; Obied et al. 2016).

Geometrically, the outflow cone is said to have an opening angle of 100° (Hjelm & Lindblad 1996) or a half opening angle of 50° with an inclination from the line of sight of 40° (Jorsater & van Moorsel 1995). From modelling the torus, Alonso-Herrero et al. (2012) estimated an opening angle of 36° . Since the torus is thought to confine the outflow opening angle, this value suggests a narrower cone. If we assume the outflow cone half opening angle of the SE cone is 36° and is inclined at 40° from the line of sight, this would limit the contribution from the direct AGN continuum. However, electrons or dust in the cone can scatter the AGN continuum. Alterna-

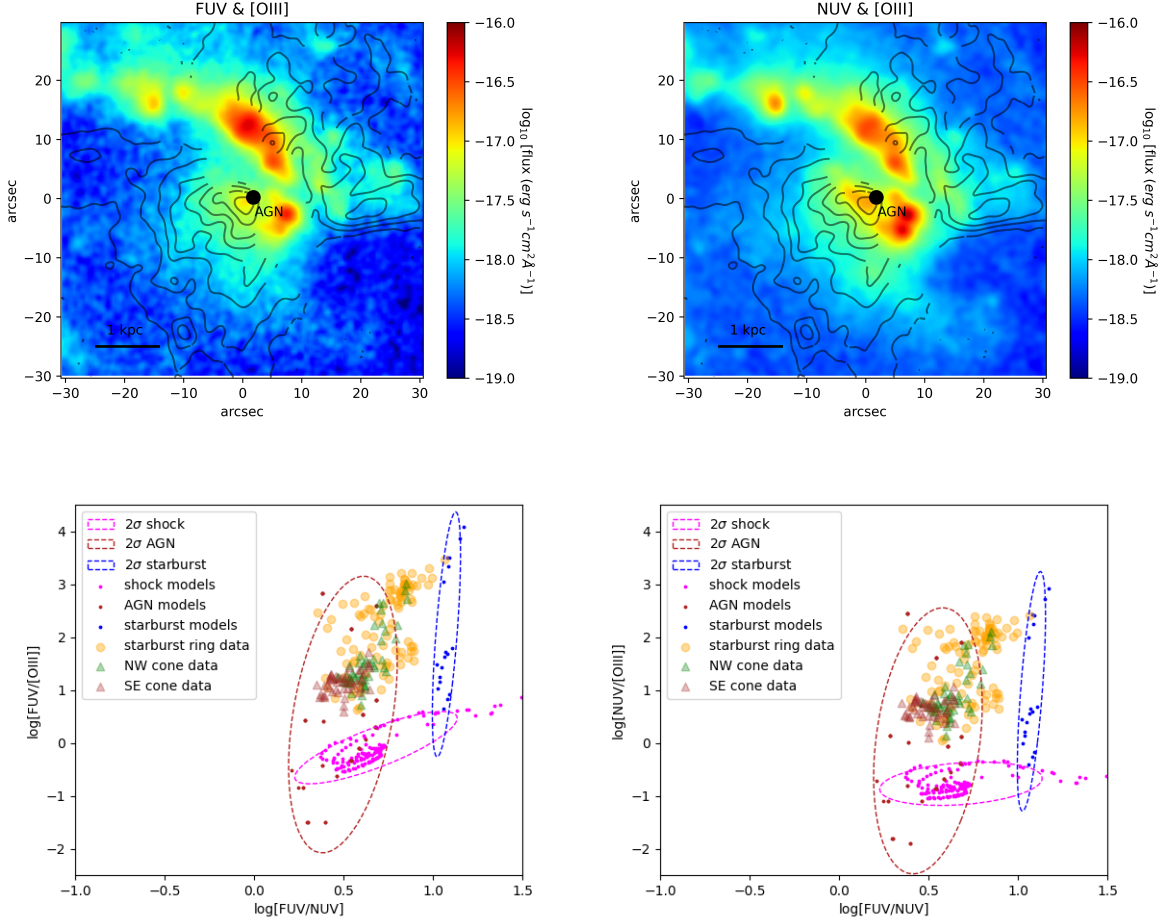


Figure 5. Results from the combined UVIT and MUSE observations: Top panel: Galactic extinction corrected FUV (left) and NUV (right) maps of the inner region of NGC 1365, with AGN dominated [OIII] 5007 Å contours from MUSE observations overlaid in black. Diffuse FUV and NUV emission is seen co-spatial to the [OIII] cone both in the NW and SE directions. Bottom panel: Flux ratios, FUV/[OIII] versus FUV/NUV (left) and NUV/[OIII] versus FUV/NUV (right) of the starburst (yellow circles), AGN NW cone (green triangles) and AGN SE cone (red triangles) in the inner region of NGC 1365. Model flux ratios of AGN and starburst photoionized gas are shown in red and blue points and shocked gas is shown in magenta. Confidence ellipses having 95% confidence are drawn around their respective model values.

tively, there can also be a contribution from two-photon decay and hydrogen fluorescence to diffuse UV emission (Kulkarni 2022). The fact that the diffuse emission is detected in both FUV and NUV, as well as in both the southern and part of the northern cones, may provide the strongest support to the scattered light origin. This is also in accord with the results found by Zakamska et al. (2005) and Obied et al. (2016) in scattering cones of AGN.

Our observations indicate that deep UV data can also be used to reveal scattered light by dust in the AGN outflow. To the best of our knowledge, such a study, combining photometric UV data with spectroscopic [OIII] emission, has not been undertaken in Seyfert galaxies and this is the first study of its kind.

4.5. Impact of AGN feedback in NGC 1365

From the estimation of the UV SFR surface density, the AGN outflow in NGC 1365 seems to have no impact on the total SFR in the circumnuclear ring as the SFR surface density is comparable to other starbursts. Also, the SFR variation seen in the central ring need not be due to the observed AGN outflow. NGC 1365 is a barred galaxy and in such galaxies, gas flows into the nuclear rings via the dust lanes. From hydrodynamical simulations, it is found that variations in the gas inflow rate can lead to changes in SF in the nuclear ring, including lopsided star formation (Sormani et al. 2023). Therefore inflow has a causal connection in regulating SF in nuclear rings (Sormani et al. 2020; Moon et al. 2021, 2022). Lopsided star formation in nuclear rings is known from observations (Callanan et al. 2021). Recent

high resolution observations of NGC 1365, supported by simulations, also favour a scenario wherein the varied SFR in the ring is due to gas inflow (Schinnerer et al. 2023). We thus conclude that the ionized AGN outflow has no impact on the molecular gas in the central region of NGC 1365 and thus the observed lopsided star formation in the ring on either side of the AGN in NGC 1365 is explainable without invoking AGN feedback (Schinnerer et al. 2023).

The ionised gas in the [OIII] outflow has velocities of the order of 100–150 km/s. (Venturi et al. 2018; this work). We estimated the escape velocity at 1 kpc to be of the order of 600 km/s using the equation in Rupke et al. (2002),

$$v_{esc}(r) = \sqrt{2} v_{circ} * [1 + \ln(1 + \frac{r_{max}}{r})]^{0.5} \quad (5)$$

where $v_{circ} = \sqrt{2} \sigma_*$ is the circular velocity and $r_{max} = 100$ kpc (Greene et al. 2011). This was calculated assuming a stellar dispersion σ_* of 120 km/s for NGC 1365 (Caglar et al. 2020). Thus, though the ionised gas is outflowing, it does not have the energy to escape the host galaxy’s potential. This is similar to the findings of other low and moderate luminosity Seyfert galaxies (Davies et al. 2014; Shimizu et al. 2019). The gas would just rain back down into the galaxy and help to relocate gas and dust and chemically enrich the galaxy. A caveat is that the outflow velocities considered here are the projected line of sight velocities and are not indicative of true outflow velocities which may be higher for high inclination angles of the outflow to the line of sight. However, Sextl et al. (2024) find low metallicities in the central region of NGC 1365 which they attribute to a combination of inflow of metal poor gas and AGN feedback interrupting the star formation in the ring. Thus, though the AGN outflow may not escape the host galaxy it may have the potential to influence the star formation in the vicinity during its active phase.

5. SUMMARY

The work presented here aims to understand the impact of AGN activity on star formation in NGC 1365 using new FUV and NUV data from UVIT combined with archival MUSE optical IFU data. The results of the work are summarised below

1. The UV data confirms existing literature studies of the SFR of the starburst ring in NGC 1365. We estimated a SFR of $2.68 M_{\odot} \text{yr}^{-1}$ for the central 2 kpc from the FUV flux map corrected for extinction using the Calzetti et al. (2000) attenuation law assuming a R_V of 3.1. The estimated SFR surface densities of NGC 1365 are similar to other starbursts.

2. We found low FUV flux values (and hence low SFR) in the east and SE part of the star forming ring (see Fig. 4 left panel). This finding based on the new UV observations reported here is in agreement with those found from the very recent high resolution observations in the infrared and sub-mm from JWST and ALMA. According to Schinnerer et al. (2023), this in-homogeneity in SF characteristics on either side of the AGN is due to differences in the onset of star formation.
3. The UV data revealed previously undetected diffuse UV emission co-spatial with the [OIII] 5007 Å outflow of AGN origin (see Fig. 5 top panel). Such a detection was possible only due to deep UV data combined with the high spatial resolution of UVIT. This points to a common origin for [OIII] 5007 Å and diffuse UV emission in the northern and southern cones.
4. Ratios of UV fluxes to [OIII] continuum subtracted line fluxes indicate that the diffuse UV emission, which is co-spatial with the [OIII] 5007 Å outflow, is of AGN origin (see Fig. 5 bottom panel). This may be due to AGN light being scattered by electrons and dust particles in the bi-cone.
5. We estimated the escape velocity at 1 kpc to be about 600 km/s. As the projected velocity of the outflowing ionised gas is much lower than the escape velocity at 1 kpc, the gas does not have the energy to escape the host galaxy potential and will rain back into the galaxy.

This work has shown the usefulness of UV in characterising the star formation nature of AGN hosts. While UV data as a direct tracer of star formation has been used extensively in star formation studies, it has been less explored in the AGN domain. With the advent of JWST, rest frame UV studies of large statistical datasets will throw new light on the prevalence of AGN feedback and its impact on host galaxies.

This publication uses data from the AstroSat mission of the Indian Space Research Organization (ISRO), archived at the Indian Space Science Data Centre (ISSDC). This publication uses UVIT data processed by the payload operations centre at IIA. The funding provided by the Humboldt Foundation, Germany is thankfully acknowledged. K.S.K. acknowledges the studentship at the European Southern Observatory, Garching. TPA acknowledges the support of the National Natural Science Foundation of China (grant nos. 12222304, 12192220 and 12192221).

Facilities: AstroSat (UVIT), VLT(MUSE). UVIT was built in collaboration between IIA, IUCAA, TIFR, ISRO and CSA.

Software: Astropy (Astropy Collaboration et al. 2013, 2018), MPDAF (Bacon et al. 2016), Cloudy 17.0 (Ferland et al. 2017)

APPENDIX

A. [OIII] AND H α FLUX MAPS

Fig. 6 shows the [OIII] and H α flux maps, we derived from the MUSE IFU data.

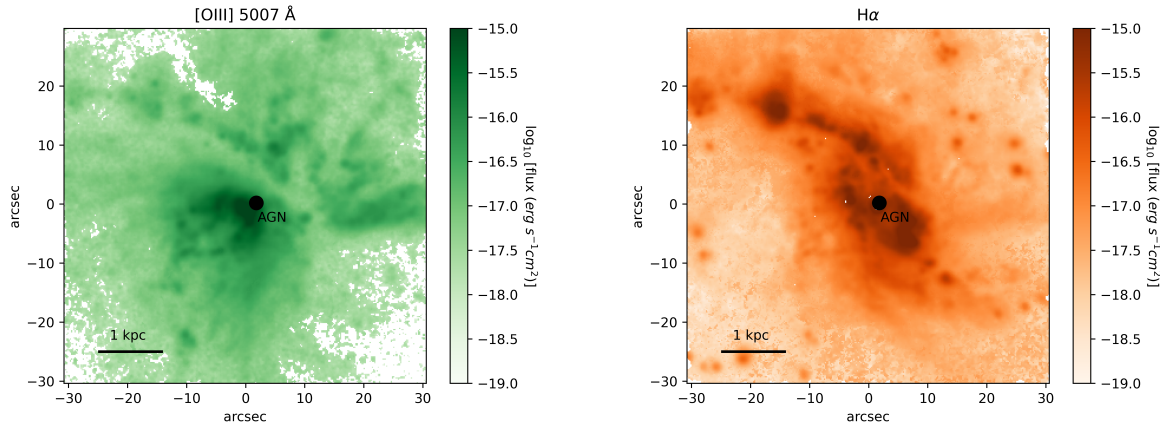


Figure 6. Flux maps of [OIII] and H α derived from the MUSE data

B. STARBURST RING AND AGN DOUBLE CONE

Fig. 7 shows the intrinsic FUV flux map with three regions of interest overlaid, from which the UV-optical flux ratios in Fig. 5 have been determined.

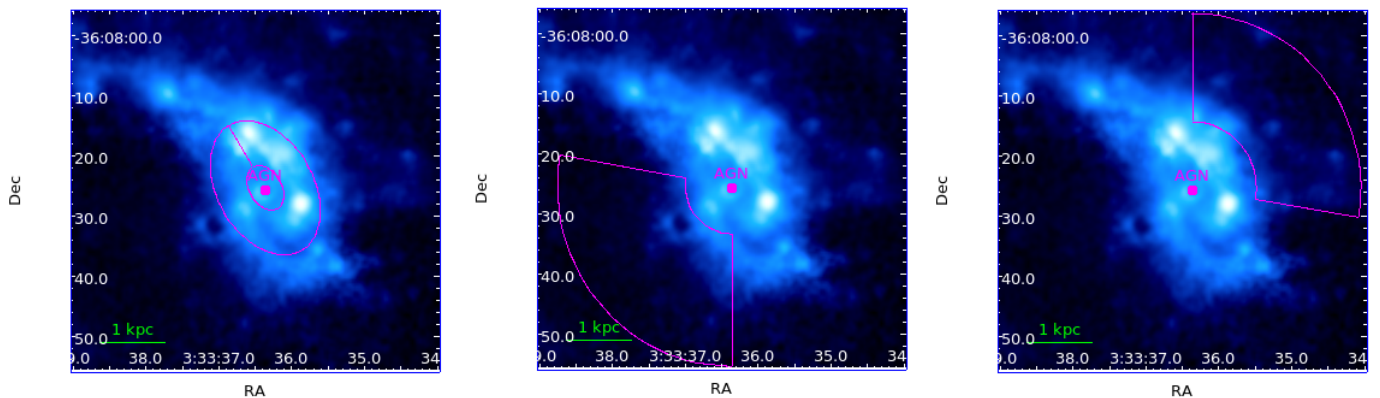


Figure 7. This figure shows the three regions used to determine the UV-optical flux ratios in Fig. 5 overlaid on the intrinsic UVIT FUV flux map. The left panel shows the 12 arcsec starburst ring after masking the central AGN. This region is also used to determine the SFR of the ring in Section 4.2. The middle and right panels show the SE and NW cones respectively.

REFERENCES

- Adhikari, T. P., Hryniewicz, K., Rózańska, A., Czerny, B., & Ferland, G. J. 2018, *ApJ*, 856, 78, doi: 10.3847/1538-4357/aab350
- Agrawal, P. C. 2006, *Advances in Space Research*, 38, 2989, doi: 10.1016/j.asr.2006.03.038

- Allen, M. G., Groves, B. A., Dopita, M. A., Sutherland, R. S., & Kewley, L. J. 2008, *ApJS*, 178, 20, doi: [10.1086/589652](https://doi.org/10.1086/589652)
- Alonso-Herrero, A., Sánchez-Portal, M., Ramos Almeida, C., et al. 2012, *MNRAS*, 425, 311, doi: [10.1111/j.1365-2966.2012.21464.x](https://doi.org/10.1111/j.1365-2966.2012.21464.x)
- Astropy Collaboration, Robitaille, T. P., Tollerud, E. J., et al. 2013, *A&A*, 558, A33, doi: [10.1051/0004-6361/201322068](https://doi.org/10.1051/0004-6361/201322068)
- Astropy Collaboration, Price-Whelan, A. M., Sipőcz, B. M., et al. 2018, *AJ*, 156, 123, doi: [10.3847/1538-3881/aabc4f](https://doi.org/10.3847/1538-3881/aabc4f)
- Bacon, R., Piqueras, L., Conseil, S., Richard, J., & Shepherd, M. 2016, *MPDAF: MUSE Python Data Analysis Framework*, Astrophysics Source Code Library, record ascl:1611.003. <http://ascl.net/1611.003>
- Baldwin, J. A., Phillips, M. M., & Terlevich, R. 1981, *PASP*, 93, 5, doi: [10.1086/130766](https://doi.org/10.1086/130766)
- Caglar, T., Burtscher, L., Brandl, B., et al. 2020, *A&A*, 634, A114, doi: [10.1051/0004-6361/201936321](https://doi.org/10.1051/0004-6361/201936321)
- Callanan, D., Longmore, S. N., Kruijssen, J. M. D., et al. 2021, *MNRAS*, 505, 4310, doi: [10.1093/mnras/stab1527](https://doi.org/10.1093/mnras/stab1527)
- Calzetti, D. 2001, *PASP*, 113, 1449, doi: [10.1086/324269](https://doi.org/10.1086/324269)
- . 2013, in *Secular Evolution of Galaxies*, ed. J. Falcón-Barroso & J. H. Knapen, 419
- Calzetti, D., Armus, L., Bohlin, R. C., et al. 2000, *ApJ*, 533, 682, doi: [10.1086/308692](https://doi.org/10.1086/308692)
- Cappellari, M., & Emsellem, E. 2004, *PASP*, 116, 138, doi: [10.1086/381875](https://doi.org/10.1086/381875)
- Cardelli, J. A., Clayton, G. C., & Mathis, J. S. 1989, *ApJ*, 345, 245, doi: [10.1086/167900](https://doi.org/10.1086/167900)
- Comerón, S., Knapen, J. H., Beckman, J. E., et al. 2010, *MNRAS*, 402, 2462, doi: [10.1111/j.1365-2966.2009.16057.x](https://doi.org/10.1111/j.1365-2966.2009.16057.x)
- Comerón, S., Salo, H., Laurikainen, E., et al. 2014, *A&A*, 562, A121, doi: [10.1051/0004-6361/201321633](https://doi.org/10.1051/0004-6361/201321633)
- D'Agostino, J. J., Poetrodjojo, H., Ho, I. T., et al. 2018, *MNRAS*, 479, 4907, doi: [10.1093/mnras/sty1676](https://doi.org/10.1093/mnras/sty1676)
- Davies, R. I., Maciejewski, W., Hicks, E. K. S., et al. 2014, *ApJ*, 792, 101, doi: [10.1088/0004-637X/792/2/101](https://doi.org/10.1088/0004-637X/792/2/101)
- Fabian, A. C. 2012, *ARA&A*, 50, 455, doi: [10.1146/annurev-astro-081811-125521](https://doi.org/10.1146/annurev-astro-081811-125521)
- Fazeli, N., Busch, G., Valencia-S., M., et al. 2019, *A&A*, 622, A128, doi: [10.1051/0004-6361/201834255](https://doi.org/10.1051/0004-6361/201834255)
- Feltre, A., Charlot, S., & Gutkin, J. 2016, *MNRAS*, 456, 3354, doi: [10.1093/mnras/stv2794](https://doi.org/10.1093/mnras/stv2794)
- Ferland, G. J., Chatzikos, M., Guzmán, F., et al. 2017, *RMxAA*, 53, 385. <https://arxiv.org/abs/1705.10877>
- Ferrarese, L., & Merritt, D. 2000, *ApJL*, 539, L9, doi: [10.1086/312838](https://doi.org/10.1086/312838)
- Galliano, E., Alloin, D., Pantin, E., Lagage, P. O., & Marco, O. 2005, *A&A*, 438, 803, doi: [10.1051/0004-6361:20053049](https://doi.org/10.1051/0004-6361:20053049)
- Gao, Y., Egusa, F., Liu, G., et al. 2021, *ApJ*, 913, 139, doi: [10.3847/1538-4357/abf738](https://doi.org/10.3847/1538-4357/abf738)
- García-Berneté, I., Alonso-Herrero, A., García-Burillo, S., et al. 2021, *A&A*, 645, A21, doi: [10.1051/0004-6361/202038256](https://doi.org/10.1051/0004-6361/202038256)
- Gordon, K. D., Clayton, G. C., Misselt, K. A., Landolt, A. U., & Wolff, M. J. 2003, *ApJ*, 594, 279, doi: [10.1086/376774](https://doi.org/10.1086/376774)
- Greene, J. E., Zakamska, N. L., Ho, L. C., & Barth, A. J. 2011, *ApJ*, 732, 9, doi: [10.1088/0004-637X/732/1/9](https://doi.org/10.1088/0004-637X/732/1/9)
- Guainazzi, M., Risaliti, G., Nucita, A., et al. 2009, *A&A*, 505, 589, doi: [10.1051/0004-6361/200912758](https://doi.org/10.1051/0004-6361/200912758)
- Harrison, C. M. 2017, *Nature Astronomy*, 1, 0165, doi: [10.1038/s41550-017-0165](https://doi.org/10.1038/s41550-017-0165)
- Hjelm, M., & Lindblad, P. O. 1996, *A&A*, 305, 727
- Ho, L. C., Greene, J. E., Filippenko, A. V., & Sargent, W. L. W. 2009, *ApJS*, 183, 1, doi: [10.1088/0067-0049/183/1/1](https://doi.org/10.1088/0067-0049/183/1/1)
- Jorsater, S., & van Moorsel, G. A. 1995, *AJ*, 110, 2037, doi: [10.1086/117668](https://doi.org/10.1086/117668)
- Kennicutt, Robert C., J. 1998, *ApJ*, 498, 541, doi: [10.1086/305588](https://doi.org/10.1086/305588)
- King, A., & Pounds, K. 2015, *ARA&A*, 53, 115, doi: [10.1146/annurev-astro-082214-122316](https://doi.org/10.1146/annurev-astro-082214-122316)
- Kormendy, J., & Ho, L. C. 2013, *ARA&A*, 51, 511, doi: [10.1146/annurev-astro-082708-101811](https://doi.org/10.1146/annurev-astro-082708-101811)
- Kormendy, J., & Richstone, D. 1995, *ARA&A*, 33, 581, doi: [10.1146/annurev.aa.33.090195.003053](https://doi.org/10.1146/annurev.aa.33.090195.003053)
- Kulkarni, S. R. 2022, *PASP*, 134, 084302, doi: [10.1088/1538-3873/ac689e](https://doi.org/10.1088/1538-3873/ac689e)
- Lang, D., Hogg, D. W., Mierle, K., Blanton, M., & Roweis, S. 2010, *AJ*, 139, 1782, doi: [10.1088/0004-6256/139/5/1782](https://doi.org/10.1088/0004-6256/139/5/1782)
- Leitherer, C., Schaerer, D., Goldader, J. D., et al. 1999, *ApJS*, 123, 3, doi: [10.1086/313233](https://doi.org/10.1086/313233)
- Lena, D., Robinson, A., Storchi-Bergmann, T., et al. 2016, *MNRAS*, 459, 4485, doi: [10.1093/mnras/stw896](https://doi.org/10.1093/mnras/stw896)
- Lindblad, P. O. 1999, *A&A Rv*, 9, 221, doi: [10.1007/s001590050018](https://doi.org/10.1007/s001590050018)
- Liu, D., Schinnerer, E., Cao, Y., et al. 2023, *ApJL*, 944, L19, doi: [10.3847/2041-8213/aca973](https://doi.org/10.3847/2041-8213/aca973)
- Magorrian, J., Tremaine, S., Richstone, D., et al. 1998, *AJ*, 115, 2285, doi: [10.1086/300353](https://doi.org/10.1086/300353)
- Maiolino, R., Gallerani, S., Neri, R., et al. 2012, *MNRAS*, 425, L66, doi: [10.1111/j.1745-3933.2012.01303.x](https://doi.org/10.1111/j.1745-3933.2012.01303.x)
- Moon, S., Kim, W.-T., Kim, C.-G., & Ostriker, E. C. 2021, *ApJ*, 914, 9, doi: [10.3847/1538-4357/abfa93](https://doi.org/10.3847/1538-4357/abfa93)

- . 2022, *ApJ*, 925, 99, doi: [10.3847/1538-4357/ac3a7b](https://doi.org/10.3847/1538-4357/ac3a7b)
- Nesvadba, N. P. H., Bicknell, G. V., Mukherjee, D., & Wagner, A. Y. 2020, *A&A*, 639, L13, doi: [10.1051/0004-6361/202038269](https://doi.org/10.1051/0004-6361/202038269)
- Obied, G., Zakamska, N. L., Wylezalek, D., & Liu, G. 2016, *MNRAS*, 456, 2861, doi: [10.1093/mnras/stv2850](https://doi.org/10.1093/mnras/stv2850)
- Osterbrock, D. E., & Ferland, G. J. 2006, *Astrophysics of gaseous nebulae and active galactic nuclei*
- Phillips, M. M., Turtle, A. J., Edmunds, M. G., & Pagel, B. E. J. 1983, *MNRAS*, 203, 759, doi: [10.1093/mnras/203.3.759](https://doi.org/10.1093/mnras/203.3.759)
- Rupke, D. S., Veilleux, S., & Sanders, D. B. 2002, *ApJ*, 570, 588, doi: [10.1086/339789](https://doi.org/10.1086/339789)
- Sandqvist, A., Hjalmarsen, Å., Larsson, B., et al. 2021, *A&A*, 647, A86, doi: [10.1051/0004-6361/202038875](https://doi.org/10.1051/0004-6361/202038875)
- Schinnerer, E., Emsellem, E., Henshaw, J. D., et al. 2023, *ApJL*, 944, L15, doi: [10.3847/2041-8213/acac9e](https://doi.org/10.3847/2041-8213/acac9e)
- Schlafly, E. F., & Finkbeiner, D. P. 2011, *ApJ*, 737, 103, doi: [10.1088/0004-637X/737/2/103](https://doi.org/10.1088/0004-637X/737/2/103)
- Sextl, E., Kudritzki, R.-P., Burkert, A., et al. 2024, *ApJ*, 960, 83, doi: [10.3847/1538-4357/ad08b3](https://doi.org/10.3847/1538-4357/ad08b3)
- Shimizu, T. T., Davies, R. I., Lutz, D., et al. 2019, *MNRAS*, 490, 5860, doi: [10.1093/mnras/stz2802](https://doi.org/10.1093/mnras/stz2802)
- Shin, J., Woo, J.-H., Chung, A., et al. 2019, *ApJ*, 881, 147, doi: [10.3847/1538-4357/ab2e72](https://doi.org/10.3847/1538-4357/ab2e72)
- Singh, K. P. 2022, arXiv e-prints, arXiv:2203.04610. <https://arxiv.org/abs/2203.04610>
- Sormani, M. C., Tress, R. G., Glover, S. C. O., et al. 2020, *MNRAS*, 497, 5024, doi: [10.1093/mnras/staa1999](https://doi.org/10.1093/mnras/staa1999)
- Sormani, M. C., Barnes, A. T., Sun, J., et al. 2023, *MNRAS*, 523, 2918, doi: [10.1093/mnras/stad1554](https://doi.org/10.1093/mnras/stad1554)
- Tandon, S. N., Subramaniam, A., Girish, V., et al. 2017, *AJ*, 154, 128, doi: [10.3847/1538-3881/aa8451](https://doi.org/10.3847/1538-3881/aa8451)
- Tody, D. 1986, in *Society of Photo-Optical Instrumentation Engineers (SPIE) Conference Series*, Vol. 627, *Instrumentation in astronomy VI*, ed. D. L. Crawford, 733, doi: [10.1117/12.968154](https://doi.org/10.1117/12.968154)
- Valencia-S., M., Zuther, J., Eckart, A., et al. 2012, *A&A*, 544, A129, doi: [10.1051/0004-6361/201219226](https://doi.org/10.1051/0004-6361/201219226)
- Veilleux, S., & Osterbrock, D. E. 1987, *ApJS*, 63, 295, doi: [10.1086/191166](https://doi.org/10.1086/191166)
- Venturi, G., Nardini, E., Marconi, A., et al. 2018, *A&A*, 619, A74, doi: [10.1051/0004-6361/201833668](https://doi.org/10.1051/0004-6361/201833668)
- Wang, J., Fabbiano, G., Elvis, M., et al. 2009, *ApJ*, 694, 718, doi: [10.1088/0004-637X/694/2/718](https://doi.org/10.1088/0004-637X/694/2/718)
- Whitmore, B. C., Chandar, R., Rodríguez, M. J., et al. 2023, *ApJL*, 944, L14, doi: [10.3847/2041-8213/acae94](https://doi.org/10.3847/2041-8213/acae94)
- Zakamska, N. L., & Greene, J. E. 2014, *MNRAS*, 442, 784, doi: [10.1093/mnras/stu842](https://doi.org/10.1093/mnras/stu842)
- Zakamska, N. L., Schmidt, G. D., Smith, P. S., et al. 2005, *AJ*, 129, 1212, doi: [10.1086/427543](https://doi.org/10.1086/427543)
- Zakamska, N. L., Hamann, F., Pâris, I., et al. 2016, *MNRAS*, 459, 3144, doi: [10.1093/mnras/stw718](https://doi.org/10.1093/mnras/stw718)
- Zubovas, K., Nayakshin, S., King, A., & Wilkinson, M. 2013, *MNRAS*, 433, 3079, doi: [10.1093/mnras/stt952](https://doi.org/10.1093/mnras/stt952)